

Highly ionized gas on galaxy scales: mapping the interacting Seyfert galaxy LEDA 135736[?]

J. Gerssen¹, D. J. Wilman², L. Christensen³, R. G. Bower⁴ and V. Wild⁵

¹Astrophysikalisches Institut Potsdam, An der Sternwarte 16, 14482 Potsdam, Germany.

²Max-Planck-Institut für Extraterrestrische Physik, Giessenbachstrasse, 85748 Garching, Germany.

³European Southern Observatory, Casilla 19001, Santiago 19, Chile.

⁴Durham University, Department of Physics, Durham, DH1 3LE, UK.

⁵Max-Planck-Institut für Astrophysik, Karl-Schwarzschild-Str. 185741 Garching, Germany

Accepted 2008 November 6

ABSTRACT

We have used the VIMOS IFU to map the properties of the Seyfert 1.9 galaxy LEDA 135736. These maps reveal a number of interesting features including: an Extended Narrow Line Region detectable out to 9 kpc, an area of intense star formation located at a projected distance of 12 kpc from the centre, an elliptical companion galaxy, and kinematic features, aligned along the long-axis of the ENLR, that are consistent with radio jet-driven mass outflow. We propose that the ENLR results from extra-planar gas ionized by the AGN, and that the AGN in turn might be triggered by interaction with the companion galaxy, which can also explain the burst of star formation and morphological features. Only about two percent of the ENLR's kinetic energy is in the mass outflow. We infer from this that the bulk of mechanical energy imparted by the jet is used to heat this gas.

Key words: galaxies:Seyfert { galaxies:interactions { galaxies:evolution { galaxies:kinematics and dynamics { galaxies:individual:LEDA 135736 { galaxies:structure.

1 INTRODUCTION

In the hierarchical picture of galaxy evolution, the formation and growth is driven by mergers. Such events affect galaxies on all scales down to their nuclei where they can trigger AGN activity (e.g. Springel et al., 2005; di Matteo et al., 2005; Cattaneo et al. 2005). Observationally, there is some evidence for a link between AGN and mergers (e.g. Sanchez et al., 2005; Kuo et al., 2008). But this connection is difficult to establish in general as the brightest AGN typically reside at redshifts too large to determine the properties of the host galaxy and its neighbours.

It is increasingly recognized, however, that feedback generated by the AGN itself plays a crucial role in galaxy evolution. A jet powered by an AGN can drive large amounts of material out of the host system and thus significantly affect its subsequent evolution. Alternatively the AGN might primarily act on the galaxy halo, heating the halo, reducing the net cooling rate and possibly expelling some material. These two modes of feedback are often referred to as the "quasar mode" and "radio mode" respectively. Models

that incorporate AGN feedback can, for instance, account for the observed galaxy luminosity functions (Croton et al. 2006, Bower et al. 2006) using the "radio mode" and can reproduce the observed M_{BH} - correlation (e.g. di Matteo et al. 2005) primarily using the "quasar mode". Observational evidence of quasar-mode feedback is emerging for intrinsically bright AGN such as QSOs (Letawe et al., 2008) and compact radio sources (Nesvadba et al., 2007; Holt et al., 2008). Meanwhile observations of X-ray cavities associated with radio sources in galaxy clusters provide clear evidence of the effectiveness of the "radio mode" (Birzan et al. 2004, Allen et al. 2006). A key issue is to observationally determine the relative importance of these two modes in lower mass systems. In this letter we present VIMOS IFU observations of a nearby, low luminosity AGN, the Seyfert 1.9 galaxy LEDA 135736 at a redshift of $z = 0.066$. The AGN in this system ionizes an Extended Narrow Line Region (ENLR) up to at least 9 kpc. Interaction with an elliptical companion, at a projected distance of 11.6 kpc, is probably triggering jet activity (as well as off-centre star formation) that we observe indirectly in the H α and [O III] kinematic maps.

[?] Based on observations made with ESO Telescopes at the Paranal Observatory under programme 078.B-0194(A).
y Email: jgerssen@aip.de

2 DATA REDUCTION AND ANALYSIS

LEDA 135736 was observed with the VIMOS Integral Field Unit (IFU) as part of a project to map the properties of a sample of 24 galaxies selected randomly from the Sloan Digital Sky Survey (SDSS; York et al. 2000). All data were obtained using the medium resolution setup (wavelength range: 5000 – 9000 Å, dispersion, 2.5 Å/pix) covering a field-of-view of 27x27 arcsec (0.67 arcsec/spaxel). We obtained two 30 minute exposures on this galaxy during service mode observations in January 2007 (in seeing conditions of about 1.5 arcsec). A detailed description of the data reduction will be given in a forthcoming paper (Gerssen et al., 2008). Briefly, we used the ESO VIMOS pipeline to perform the basic reduction steps up to spectrum extraction and wavelength calibration. The post-processing steps (e.g. throughput correction, flux calibration, and exposure combination) to create the final data cube (x, y, λ) were performed using custom written IDL scripts.

To analyse the emission line data, we independently fit the H + [N II] group, the [O III] doublet, the [S II] doublet and the H α emission line. Each line is fit with a single Gaussian, and for each set of lines the relative position and widths of each line are fixed to each other as they trace the same kinematics. For example, in a three component fit to the H + [N II] emission lines we tie the centroids and line widths to the H α line. In this case there are six free parameters: the amplitudes of the three emission lines, the line centroid and line width, and a constant continuum level. We do not include an additional broad H α component in the emission line analysis. The Broad Line Region (BLR) in LEDA 135736 is only detectable in the H α line and then only in spectra close to the nucleus, where it is so broad as to have no influence on the fit.

3 RESULTS

The galaxy LEDA 135736 is a Seyfert 1.9 at a distance¹ of 293 Mpc. Its basic properties are listed in Table 1. It stands out in our sample because the radial dependence of its strongest emission lines (H α , H β , [N II]6584 [O III]5007) indicates a high ionization state out to large radii, see Figure 1. In this so-called BPT diagram (Baldwin et al. 1981) we plot results derived using a synthetic annulus-aperture (2 arcsec width) of increasing radius. Remarkably, LEDA 135736 is located on the AGN ‘wing’ of the BPT diagram out to a radius of at least 9 kpc. This implies a role for strong ionizing radiation, probably associated with the AGN, on galaxy-wide scales.

3.1 Morphology

LEDA 135736 displays a complex morphological structure that is strongly wavelength dependent. A composite colour image derived from our data cube is shown in panel (a) of Figure 2. The two brightest knots, labelled A and B, coincide respectively with the nucleus of the host and that of a nearby galaxy. Their projected separation is 11.6 kpc. Hence, it is

Table 1. Properties of LEDA 135736

Basic		
RA (J2000)	09h59m 39.8s	
Dec (J2000)	+ 00d35m 14s	
Type	Sy 1.9	
z	0:066	
Lum inosity		
L_X (erg s ⁻¹)	7:2	10 ⁴²
$L_{[O III]}$ (erg s ⁻¹)	4:2	10 ⁴⁰
L_H (erg s ⁻¹)	4	10 ⁴⁰
$L_{1.4GHz}$ (erg s ⁻¹ Hz ⁻¹)	7:7	10 ²⁹

likely that the two systems are interacting. A clear manifestation of interaction are the faint knots visible NE of the host nucleus. The knot labelled C coincides with the peak of a resolved ultraviolet source (GALEX database). The H α and [O III] line flux maps (panels d and g) respectively do show prominent features in region C as well. Interestingly, the H α peak intensity is somewhat stronger for the off-centre peak than on the nucleus itself. The average line ratios over region C (shown in Figure 1) are consistent with ionization by young stars. This area is likely associated with off-centre star formation (at 10.8 projected kpc from the nucleus) triggered by interaction with the companion galaxy.

As the companion galaxy shows no emission lines we establish its nature using a near infrared H-band image obtained from the UKIRT Infrared Deep Sky Survey (UKIDSS; Lawrence et al. 2007). The surface brightness profile (derived with ELLIPSE in IRAF) is consistent with the light profile of an elliptical galaxy with an effective radius of $R_e = 2.5$ kpc.

3.2 Stellar kinematics

To constrain the systemic velocities of the host and the companion we sum the spectra in our data cube over regions A and B. We use the pixel-fitting method of (Cappellari & Emsellem 2004) to fit the summed spectra with a set of stellar template spectra observed with EMMI on the NTT (convolved to the VIMOS instrumental resolution of 7.3 Å). The comparison, shown in panel (b), between the stellar absorption line spectra extracted at locations A and B demonstrates that the companion galaxy is also close in velocity space ($v_{los} = 600$ km s⁻¹).

3.3 Extended Narrow Line Region

To examine the result shown in Figure 1 in more detail we can use our data cube to derive the line ratios in each spatial element individually. The full 2-D line ratio map of [O III] 5007/H α is shown in panel (c) of Figure 2. Consistent with our azimuthally averaged result (Fig. 1), the map shows an extended region of highly ionized gas. The observed line ratios require a very strong ionization field (hard UV spectrum) and are typical for the Narrow Line Region (NLR) of a Seyfert galaxy. Such highly ionized gas, not confined to the nuclear regions of a galaxy, is known as an Extended Narrow Line Region (ENLR) (e.g. Bennert et al., 2006). As the overplotted contours demonstrate, the spatially resolved

¹ The luminosity distance is calculated assuming: $H_0 = 0.73$, $H_0 = 0.27$, $H_0 = 71$ km s⁻¹ Mpc⁻¹. The scale is 1.25 kpc/arcsec.

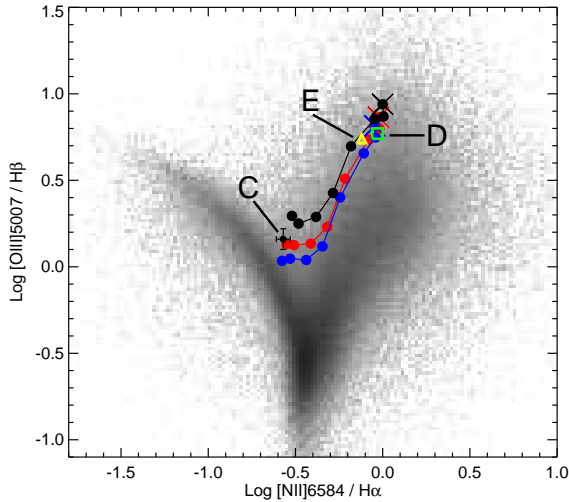


Figure 1. To broadly quantify the radial dependence of the properties of LEDA 135736 we measure emission line fluxes in annuli of increasing radius. The result is shown as a ‘track’ (black line) on top of a BPT diagram derived from single-aperture measurements of some 500,000 galaxies in the SDSS database (Brinchmann et al. 2004). Our central aperture ($1''$ radius) is indicated by the cross. The radius increases by $2''$ for successive points along the track. Standard corrections for Balmer absorption of $EW = 2 \text{ \AA}$ and $EW = 4 \text{ \AA}$ (red and blue coloured tracks respectively) do not significantly change the results. The location of the off-centre star-forming region (region C, see section 3.1) in this diagram is marked by the black square with error bars and is corrected for stellar absorption ($EW = 2 \text{ \AA}$). The 1 σ errors on the azimuthally-averaged measurements are smaller than the symbol sizes. The open square and triangle show the line ratios in box D & E respectively (section 4).

part ($\sim 5 \text{ kpc}$) of the ENLR in LEDA 135736 is somewhat elongated ($a > b > 2$) with the long axis at a PA $\sim 45^\circ$.

Panels (d) and (e) of Figure 2 respectively show the H flux and velocity field. The Balmer lines are relatively more sensitive to less strongly ionized radiation fields than the $[\text{O III}]$ line (as utilised by the BPT diagram) and so more closely traces gas ionized by young stars. The rotating disk traced by the H line is therefore probably unrelated to the ENLR, with gas ionized by normal star formation in the disk. Our radially-averaged results (Fig. 1) illustrate that out to $\sim 9 \text{ kpc}$ the $[\text{O III}]$ line includes contributions from both disk gas ionized by young stars, and the more highly ionized gas from the AGN (the ENLR). Beyond $\sim 9 \text{ kpc}$ (including region C) star formation dominates, and the line ratios are consistent with normally star-forming galaxies.

3.4 Gas kinematics

The gas kinematics derived from the H and $[\text{O III}]5007$ emission lines are shown in Figure 2 along the middle row and bottom row respectively. The average error on the best-fit (as described in section 2) line centroids and line widths is $\sim 10 \text{ km s}^{-1}$.

On a global scale the H velocity field (panel e) is consistent with a simple rotating disk model. Near the systemic velocity, however, the data are significantly distorted from the straight line zero velocity contour (green in our map)

predicted by this model. The peak in the H velocity dispersion map (panel f) does not coincide with the nucleus itself but is located SE of it along the long-axis of the ENLR in a region that we label D. Interestingly, a second dispersion peak, labelled F, is visible in the direction of the companion galaxy. The off-centre dispersion peaks cannot be attributed to an unaccounted for broad line component as they are located well beyond the BLR.

The $[\text{O III}]$ kinematic maps (panels h & i) also show pronounced features in the off-centre region D. The observed velocity blob in this region is offset from the systemic velocity by about 150 km s^{-1} and is located too far from the galaxy centre ($\sim 5 \text{ kpc}$) to be related to the kinematics of the nucleus itself.

3.5 Other Wavelengths

LEDA 135736 has been detected in X-ray and Radio wavelengths at values typical for a Seyfert galaxy. Anderson et al. (2003) associate this system with an X-ray source in the ROSAT All Sky Survey (RASS) of $\log_{10} (L_X / \text{erg s}^{-1}) = 42.86$. From the NVSS 1.4 GHz radio survey we derive a total luminosity of $7.7 \times 10^{22} \text{ W Hz}^{-1}$. The more accurate position and better resolution of the FIRST 1.4 GHz survey shows that this radio source is centred on the host galaxy nucleus, coincident with the ENLR. It appears to be unresolved in these data implying an upper limit on its projected size of 7.2 kpc (see Fig. 2 panel h).

4 DISCUSSION AND CONCLUSIONS

The high ionization state of the ENLR (with a ratio $[\text{O III}]/\text{H}$ in the range 5–10) is suggestive of gas photo-ionized by the AGN. Ionization from star formation is not so hard, and shocks also tend to produce lower line ratios (Villar-Martin et al. 1999). With a radius along its long axis of $\sim 9 \text{ kpc}$ the ENLR is quite large. However, larger ENLRs extending up to 20 kpc in Seyfert galaxies have been observed before (Unger et al. 1987; Fraquelli et al. 2000). In order for the AGN ionizing radiation to reach such radii, the AGN ionization cone must be pointing out of the galaxy disk and excite the extra-planar gas (Storchi-Bergmann et al. 1992). The presence of this gas and its observed high velocity dispersion suggests kinematic heating by the AGN.

The detailed correspondence between features in radio maps and emission line images of Sy 2 galaxies suggest strong interactions between the radio jets and the ENLR (e.g. Falcke et al. 1998; Villar-Martin et al. 1999). Hence, the blob of perturbed kinematics in LEDA 135736 (region D in Fig. 2) at $\sim 5 \text{ kpc}$ from the nucleus along the ENLR axis is expected to be closely aligned with the radio structure. Although we cannot discard alternative scenarios, an interesting possibility is that the kinematic perturbation has been triggered by interaction with the radio structures.

In this interpretation the observed kinematics reflect material being driven out by the jet. The impact of such an outflow on the surrounding medium stirs up the gas, presumably by the vortices trailing the jet shock-front, leading to large (random) gas motions. A caveat here is that the observed kinematics could also be attributed to gas falling into the nucleus (possibly as the result of the interaction

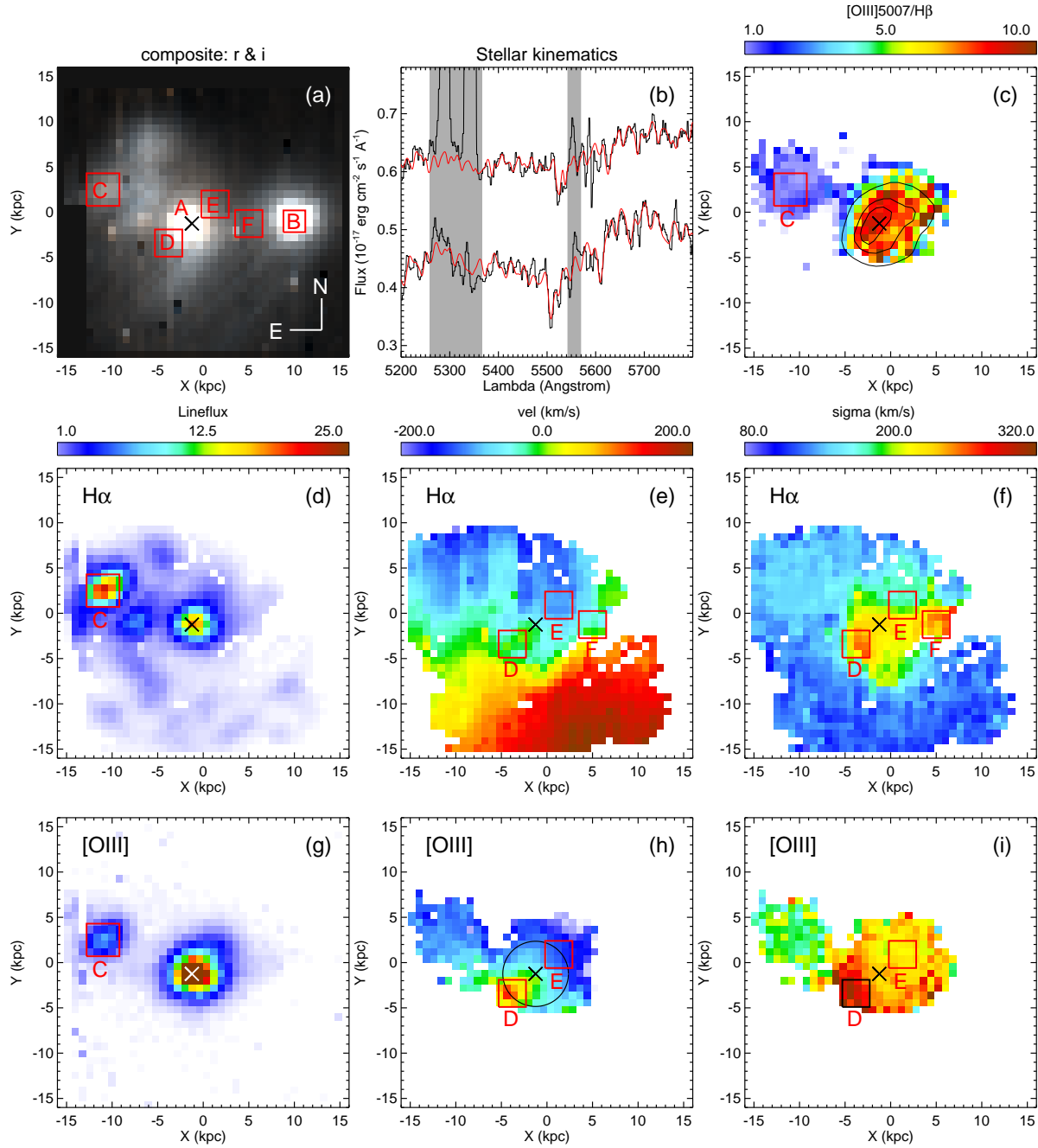


Figure 2. Properties of LEDA 135736 derived from the VIMOS IFU data. In all panels the orientation is such that North is up and East is the left. The position of the Broad Line Region, and hence the nucleus itself, is marked with the cross in each panel. Top row : a : A composite image created by emulating the SDSS r- and i-band filter profiles. The labelled regions (A to F) are discussed in detail in the text. b : Absorption line spectra of the companion galaxy (bottom curve) summed over the box labelled B in panel (a). The top curve shows the spectrum of the host galaxy summed over a similar sized area. The spectra are plotted over a wavelength range around the Mg b stellar absorption line feature ($\lambda = 5170 \text{ \AA}$) with single stellar template spectra. The best fits are shown in red. The wavelength contaminated by emission lines are excluded in this plot (dashed regions). c : Ionization map. The high values $f_{[\text{OIII}] 5007} = f_{\text{H}} \gg 1$ suggest an AGN as the source of ionization. The orientation of this Extended Narrow Line Region is highlighted by the overplotted contours. Its long axis lies along a position angle of 45° . In this and subsequent panels the colour map scales are linear. Results are shown only for spaxels with line flux S/N ratios > 3 . Middle row : Maps of the H α line flux, the H α velocity field, and the velocity dispersions. The labelled boxes (C : α -centre SF region, D : α -centre velocity dispersion peaks) are discussed in detail in the text. Bottom row : Similar to the middle row but showing the [OIII]5007 properties on the same scales as the H α properties. The black circle in panel (h) delineates the upper limit on the size of the unresolved radio source.

with the companion galaxy). However, in that scenario it is difficult to explain the high velocity dispersion of the gas.

It is interesting to note that on the opposite side of the nucleus (region E) neither the H α nor the [O III] kinematic maps show any remarkable features. The ionization state, however, is similar to region D. The H α dispersion map does show a large perturbation in region F. Perhaps this is the signature of the counter jet although it could also be due to interaction with the companion galaxy.

The total [O III] luminosity that we derive from the flux distribution shown in panel (g) is 4.2×10^{40} erg s $^{-1}$ (ignoring the contribution from region C, which is due to star formation). This is equivalent to the H α luminosity of the ENLR, $L_{\text{H}\alpha} = 4 \times 10^{40}$ erg s $^{-1}$. Note that this will include the contribution from the gas disk, which cannot be properly separated from the highly ionized extra-planar gas. In comparison, the mechanical power of the jet itself can be estimated using an empirical conversion from radio luminosity (equation (1) of Best et al. 2007). The observed radio flux (table 1) implies $L_{\text{mech}} = (4 \pm 2) \times 10^{42}$ erg s $^{-1}$, roughly an order of magnitude more than the energy which is reradiated as emission lines. The X-ray luminosity (table 1) is larger than both L_{mech} and the emission line luminosities (H α and [O III]) as expected (e.g. Heckman et al. 2004).

If we assume that most of the mechanical energy of the jet is converted to kinetic energy in the extra-planar gas then we can compute an upper limit on the mass of ionized hydrogen in the ENLR. Over the lifetime of the jet, $\sim 10^6$ yr (e.g. Sanders 1984), the upper limit on the available energy in the ENLR is: $\sim 4 \times 10^{42}$ erg s $^{-1} \times 10^6$ yr $\sim 1.3 \times 10^{56}$ erg. The jet lifetime is also consistent with its small size of ~ 5 kpc, assuming a canonical jet velocity of $\sim 0.1c$. With the typical gas velocities observed in our data of $V_{\text{RMS}}^2 = V_{\text{rot}}^2 + \sigma^2 \sim 300$ km s $^{-1}$, this kinetic energy would correspond to an upper limit on the mass in ionized hydrogen of $\sim 1.4 \times 10^8 M_{\odot}$.

In our interpretation, we associate the structure observed in region D with jet driven mass outflow. The fraction of the total kinetic energy needed to power this outflow is simply the fraction of mass in region D multiplied by the ratio of the bulk velocity (~ 150 km s $^{-1}$) to $V_{\text{RMS}} \sim 300$ km s $^{-1}$ squared. Under the assumption of constant gas density, the fraction of mass can be estimated as the fraction of [O III] luminosity in region D, ~ 0.07 . Therefore the fraction of ENLR kinetic energy in this bulk outflow is $1.3 \times 10^{56} \times 0.07 \times (150/300)^2 \sim 2.3 \times 10^{54}$ erg. That is, only about 2 percent of the mechanical energy is required to power the outflow.

The derived energies are order of magnitude estimates only but are all internally consistent. The low mass loading and velocity associated with the outflow makes it unlikely that this process has a profound impact on the cold gas content of this galaxy. However, the implied mechanical energy of the jet is 50 times greater | on this basis only a small fraction of the jet energy is used to power the outflow. A much larger fraction is available to heat the gas which we observe as the highly ionized, large ENLR in this galaxy. It is notable that the jet energy is comparable to the cooling luminosity of a 1 keV ($\sim 10^{13.5} M_{\odot}$) halo. This is an important point | in this galaxy feedback from the AGN seems to have little direct effect on the galaxy: any influence it can have occurs through the heating of gas in the galaxy's halo.

This scenario is very much consistent with current galaxy formation models (e.g., Croton et al. 2006, Bower et al. 2006, 2008). Compared with powerful QSOs (e.g. Nesvadba et al. 2007) and radio galaxies (e.g., Best et al. 2007) the jet energy is small. Nevertheless, it is the impact of AGN feedback in 10^{12} ($10^{13} M_{\odot}$) haloes that is responsible for shaping the galaxy luminosity function.

The jet of this low mass AGN in part smoothes its kinetic energy into the cold gas by means of kinetic heating than by directed outflow. IFU observations of galaxies hosting radio AGN, such as presented in this letter, provide key insight into the coupling between the jet and the gas.

ACKNOWLEDGMENTS

We thank the referee, Montserrat Villar-Martin, for the constructive comments and suggestions. We also like to thank Chris Done, Isabelle Gavignaud, Martin Krause and Marc Schartmann for helpful discussions.

REFERENCES

- Allen, S. W., R. J. H. Dunn, Fabian, A. C., Taylor, G. B., & Reynolds, C. S. 2006, MNRAS, 372, 21
- Anderson, S. F., Voges, W., Morgan, B., Trumper, J., Agueros, M. A., Boller, T., Collinge, M. J. et al. 2003, AJ, 126, 2209
- Baldwin, J. A., Phillips, M. M., Terlevich, R. 1981, PASP, 93, 5
- Bennert, N., Jungwirth, B., Komossa, S., Haas, M., & Chini, R. 2006, A&A, 456, 953
- Best, P. N., von der Linden, A., Kaumann, G., Heckman, T. M., & Kaiser, C. R. 2007, MNRAS, 379, 894
- Bower, R. G., Benson, A. J., Malbon, R., Helly, J. C., Frenk, C. S., Baugh, C. M., Cole, S. & Lacey, C. G. 2006, MNRAS, 370, 645
- Bower, R. G., McCarthy I. G., Benson A. 2008, MNRAS, submitted
- Brinchmann, J., Charlot, S., White, S. D. M., Tremonti, C., Kaumann, G., Heckman, T. & Brinchmann, J. 2004, MNRAS, 351, 1151
- Cappellari, M. & Emsellem, E. 2004, PASP 116, 138
- Cattaneo, A., Combes, F., Colombi, S., Bertin, E. & Melchior, A.-L. 2005, MNRAS, 359, 1237
- Croton, D. J., et al. 2006, MNRAS, 365, 11
- Di Matteo, T., Springel, V. & Hernquist, L. 2005, Nat, 433, 604
- Falcke, H., Wilson, A. S. & Simpson, C. 1998, ApJ, 502, 199
- Fraquelli, H. A., Storch-Bergmann, T. & Binette, L. 2000, ApJ, 532, 867
- Heckman, T. M., Kaumann, G., Brinchmann, J., Charlot, S., Tremonti, C., & White, S. D. M. 2004, ApJ, 613, 109
- Holt, J., Tadhunter, C. N. & Morganti, R. 2008 arXiv:0802.1444v1
- Kuo, C.-Y., Lin, J., Tang, Y.-W., & Ho, P. T. P. 2008 (arXiv:0802.4205v1)
- Lawrence, A. et al. 2007, MNRAS, 379, 1599
- Letawe, Y., Magain, G., Letawe, G., Corbin, F. & Hutsemekers, D. 2008 arXiv:0802.1386v1

- Nesvadba, N. P. H., Lehnert, M. D., De Breuck, C., Gilbert, A. & van Breugel, W. 2007, *A & A*, 475, 145
- Sanders, R. H. 1984, *A & A*, 140, 52
- Sanchez, S. F., Becker, T., Garcia-Lorenzo, B., Benn, C. R., Christensen, L., Kelz, A., Jahnke, K. & Roth, M. M. 2005, *A & A*, 429L, 21
- Springel, V., Di Matteo, T., & Hernquist, L. 2005, *MNRAS*, 361, 776
- Storch-Bergmann, T., Wilson, A. S. & Baldwin, Jack A. 1992, *ApJ*, 396, 45
- Unger, S. W., Pedlar, A., Axon, D. J., Whittle, M., Meurs, E. J. A. & Ward, M. J. 1987 *MNRAS*, 228, 671
- Villar-Martin, M., Tadhunter, C., Morganti, R., Axon, D. & Koekenker, A. 1999, *MNRAS*, 307, 24
- York, D. G. et al. 2000, *AJ*, 120, 1579